Journal of Materials Chemistry A

Accepted Manuscript

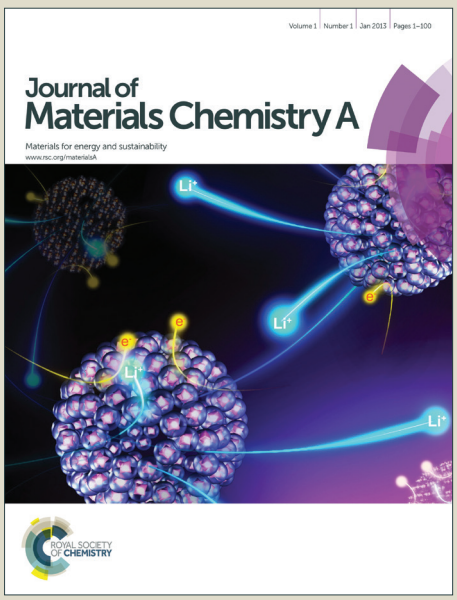

ROYAL SOCIETY OF CHEMISTRY

www.rsc.org/materialsA

Rigid Bolaform Surfactant Templated Mesoporous Silicon Nanofibre for Anode Material of Lithium-Ion Batteries

Dongpo Xu, Zhehao Huang, Rongrong Miao, Yitian Bie, Jun Yang*, Yuan Yao* and Shunai Che*

Received (in XXX, XXX) Xth XXXXXXXXX 20XX, Accepted Xth XXXXXXXXX 20XX00
DOI: 10.1039/b000000x

Mesoporous silicon nanofibres were synthesised by magnesiothermic reduction of earthworm-like, lamellar structured silica nanotubes for use in developing highly efficient lithium ion batteries. The silica nanotubes resulted from the single-molecular-layer arrangement of a bolaamphiphile surfactant. The calcined mesoporous silica nanotubes transformed into mesoporous silicon nanofibres (nf-Si) after magnesiothermic reduction. Finally, carbon-layer-coated silicon nanofibres (nf-Si@C) were obtained by chemical vapour deposition (CVD), which displayed a stable capacity of approximately 1141 mAh g^{-1} over 100 cycles at 0.2 C.

Introduction

Lithium-ion batteries are very important power sources for energy storage and other applications because of their high energy density, excellent cycling performance, designability and environmental friendliness[1-3], but commercial graphite anode lithium-ion batteries connot meet the increasing requirements for high performance due to their low theoretical capacity (372 mAh g^{-1}) and poor rate capability[4, 5]. Silicon-based materials are regarded as the most promising candidate for replacing graphite as anode materials owing to their extremely high theoretical capacity (4200 mAh g^{-1}, ca.$Li_{4.4}Si$)[6, 7]. However, silicon suffers from serious capacity fade and pulverisation due to volume swings during lithium-ion insertion/extraction, which represents an obstacle in applying silicon as an anode material[7-10].

Recently, three basic strategies have been proposed to overcome the aforementioned problems: reducing the alloy particle size, using silicon composites and introducing porous silicon structures [11-14]. Most of the these silicon materials can be synthesised by physical methods such as vapour-liquid-solid growth[15], chemical vapour deposition (CVD) of amorphous silicon or SiH_4[16] and supercritical fluid-liquid-solid (SFLS)[17]. For example, Holzapfel et al. prepared a silicon-graphite composite with a stable capacity of 1000 mAh g^{-1} as a lithium anode material[14]. Liu's group reported carbon-coated, 44 wt.% silicon nanocomposites with a capacity of 1489 mAh g^{-1} after 20 cycles[18]. Cui's group reported a series of silicon materials used as high-performance lithium-ion battery anodes, including silicon nanospheres[19], nanotubes[16, 20], and nanowires[17]. However, the electrochemical performance of silicon must be further improved to achieve higher capacity, higher coulombic efficiency and better cyclability. However, the physical synthesis methods currently employed limit the application of silicon materials due to the large equipment investment.

The porous structure has been demonstrated to be an effective means of accommodating the volume expansions/contractions[10, 19, 21, 22] of silicon because it provides sufficient space to absorb large volume expansions and thereby enhances the electrochemical performance. Wang's group reported a series of porous silicon materials used as high-performance lithium-ion battery anodes[23, 24]. Porous-structured silicon can be conveniently obtained through the magenesium reduction of ordered mesoporous silica directed by the self-assembly of small molecules or block copolymer templates[25, 26]. After being coated with a thin carbon layer, the mesoporous silicon materials obtained in this manner have been reported to show excellent electrochemical performance [9].

Herein, we report the synthesis of mesoporous silicon nanofibres templated by a rigid bolaform amphiphilic surfactant for lithium- based energy storage. The rigid amphiphilic bolaform surfactant (Figure 1a) was designed and synthesized as a template capable of forming micelles with a lamellar arrangement in aqueous solution due to its special structure, which features a rigid benzenone ring in the middle and hydrophilic carboxylic acids at the both ends. Silica nanotubes with an earthworm-like, lamellar interior were synthesised through the co-structure directing route (Figure 1b) [26]. The carboxylic acids at the two ends of the surfactant interact electrostatically with the amino group of 3-aminopropyltrimethoxysilane (APS), and the alkoxysilane sites of APS are co-condensed with tetraethylorthosilicate (TEOS) to form a silica framework. Pure silica nanotubes were prepared by calcination (Figure 1c). Silicon nanofibre (nf-Si) structures with accumulated silicon nanoparticles were obtained by magnesiothermic reduction and subsequent magnesium oxide etching (Figure 1d). The CVD method was employed to coat a very tin carbon layer on the surface of the mesoporous silicon nanofibres (nf-Si@C) to enhance the surface electric conductivity and stabilize the morphology and structure of the nanofibres for use as an anode material (Figure 1e) .

School of Chemistry and Chemical Engineering, State Key Laboratory of Metal Matrix Composites, Shanghai Jiao Tong University, 800 Dongchuan Road, Shanghai, 200240 (P. R. China) E-mail: chesa@sjtu.edu.cn; yangj723@sjtu.edu.cn; yaoyuan@sjtu.edu.cn.

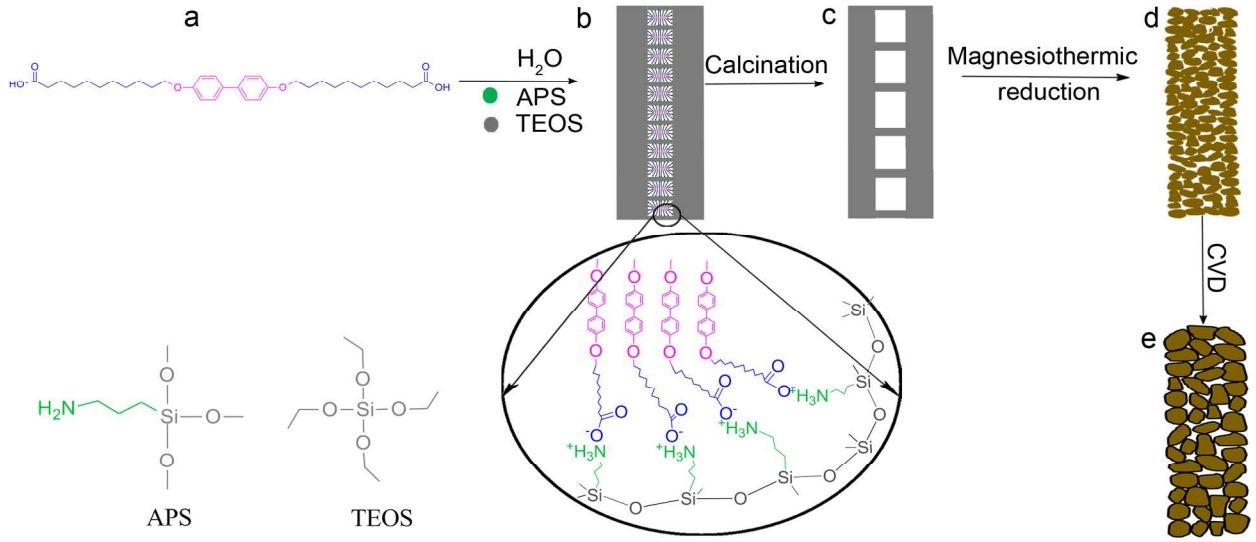

Fig. 1 Schematic illustration of the formation of nf-Si@C. (a) Molecular structural formula of the rigid bolaform surfactant, (b) a layered structural silica nanotube with the lamellar arrangement of the bolaform surfactant, (c) a calcined silica nanotube after removing the surfactant, (d) the nf-Si with accumulated silicon nanoparticles, (e) the nf-Si@C with the silicon nanoparticles covered with a thin carbon layer.

Experimental

Materials

11-Bromoundecanoic acid (98% Aladdin), 4,4'-dihydroxybiphenyl (99% J & K Scientific), APS (98%, TCI) hydrochloric acid (HCl, 36%, Sinopharm Chemical Reagent Co., Ltd), sodium hydroxide (Sinopharm Chemical Reagent Co., Ltd), anhydrous ethanol (Sinopharm Chemical Reagent Co., Ltd) and TEOS (98%, TCI) were purchased and used as received. Millipore-Q water (18 MΩcm) was used in all experiments.

Methods

Synthesis of surfactant

The surfactant was synthesised to have the following molecular formula: HOOC-$C_{10}H_{20}$-O-ph-ph-O-$C_{10}H_{20}$-COOH. 4,4'- Dihydroxybiphenyl (9.3 g, 0.05 mol) was dissolved in 300 mL ethanol. Then, 70 mL of a NaOH (8.4 g, 0.21 mol) ethanol solution was added, and the mixed solution was stirred for approximately 30 min. 11-Bromoundecanoic acid (27.83 g, 0.105 mol) was added under stirring, and the mixture was refluxed at 95 °C under a N_2 atmosphere for 5 h. The product was filtered and washed repeatedly with 1.5 L of 60 °C hot water for several times, and finally dried under vacuum.

^{1}H-NMR (400 MHz, DMSO-d_6), δ(ppm): 11.96 (s, 2H, -COO**H**), 7.48-7.50 (d, J(H,H) = 8 Hz, 4H, -C_6**H**$_4$-C_6**H**$_4$-), 6.94-6.96 (d, J(H,H) = 8 Hz, 4H, -C_6**H**$_4$-C_6**H**$_4$-), 3.96 (t, 4H, -C**H**$_2$OPh-PhOC**H**$_2$-), 1.21-2.18 (m, 36H, attaching to the long alkyl chain).

Synthesis of silica nanotubes with lamellar structure

The surfactant was dissolved in sufficient water and stirred for 30 min at 80 °C to form a clear solution. APS and TEOS were then added to the clear solution with stirring. The molar ratios of the resulting gels were 1Surf : 14APS : 14TEOS : 22000H_2O. The mixture was kept at 80 °C while stirring for 2 h and then aged for 2 days at 80 °C. The product was filtered and washed repeatedly with water for several times and finally freeze-dried to obtain as-synthesised silica nanotubes. The template was removed by calcination at 550 °C for 6 h.

Synthesis of mesoporous nf-Si

The calcined silica nanotubes (0.4 g) and magnesium powder (0.34 g, 100 ～ 200 mesh) were placed in a corundum boat and then heated in a tube furnace at 650 °C for 4 h under an Ar (95 vol.%)/H_2 (5 vol.%) mixed atmosphere. The heating speed was maintained at 2 °C min^{-1}. The brown powder obtained was immersed in HCl solution (20 mL, 2 M) for 12 h and then washed with distilled water and ethanol by centrifugation 4 times. The products were finally vacuum-dried at 80 °C for 2 h.

Fabrication of mesoporous nf-Si@C

The nf-Si particles were coated with carbon via a CVD method by using toluene as the carbon source. The CVD process was carried out at 800 °C for 30 min under a high-purity argon atmosphere to obtain nf-Si@C.

Characterisation

The morphologies of the samples were observed by scanning electron microscopy (SEM, JEOL JSM-7401F) at 1.0 kV. Transmission electron microscopy (TEM) was performed using a JEOL JEM-2100 microscope operated at 200 kV. N_2 adsorption–desorption isotherms were obtained at 77 K on a Quadrasorb SI automated surface area and pore size analyser. The pore-size distribution curves were calculated by the Barrett–Joyner–Halenda (BJH) method by using the desorption branch of the isotherms. Powder XRD patterns were recorded on a Rigaku X-ray diffractometer D/MAX-2200/PC equipped with a Cu KR radiation source (35 kV, 200 mA) at a rate of 1°/min over the range of 1-6° (2θ). ^{1}H NMR spectra were recorded on a Varian MERCURY plus-400 (400 MHz) spectrometer, and the chemical

shifts were reported in ppm relative to the residual deuterated solvent and the internal standard tetramethylsilane.

Cells assembly and electrochemical testing

Electrochemical experiments were carried out by using CR2016-type coin cells with an ENTEK ET20-26 membrane as the separator and lithium foil as the counter electrode. The electrolyte was 1 M $LiPF_6$ in a mixture of ethylene carbonate (EC) and dimethyl carbonate (DMC) (1:1 in volume ratio), plus 2 wt.% vinylene carbonate (VC). The working electrode consisted of 60 wt.% silicon-based active material, 20 wt.% conducting agent (Super P) and 20 wt.% binder (styrene butadiene rubber/sodium carboxymethyl cellulose, 1:1 by weight).The cells were assembled in an argon-filled glove box (MBRAUN Unilab, Germany) with oxygen and water contents less than 10 ppm. The electrochemical performance of the cells was evaluated on a LAND battery test system (Wuhan Kingnuo Electronics Co., Ltd., China) at 25 °C. The cut-off voltage was 0.01 V versus Li/Li^+ for discharge (Li insertion) and 1.2 V versus Li/Li^+ for charge (Li extraction). The specific capacity was calculated based on the total composite weight.

Result and discussion

Figure 2 presents SEM and TEM (a, b, c, d) images of the samples synthesized by self-assembly of the bolaform surfactant, APS and TEOS. Figure $2a_2$ shows the silica nanotubes with lamellar-structured interiors. The average inner diameter, wall thickness and interlayer spacing were ~80, ~33 and ~4.4 nm, respectively. After calcination, silica nanotubes measuring ~77 nm in diameter were formed, in which the layers at the centre collapsed and overlaid together due to the removal of the template (Fig. 2b). Following the magnesiothermic reduction and etching process, the nanotubes still maintained their primary morphology (Fig. $2c_1$). However, the layers in the interior of the nanotubes collapsed into solid fibres (~88 nm) with accumulated silicon nanoparticles (Fig. $2c_2$). The conversion of silica to silicon was later confirmed by X-ray diffraction (XRD). The TEM images shown in the inserts and the selected area electron diffraction (SAED) spots of the nf-Si show the polycrystalline nature of the silicon, indicating that disordered mesoporous nf-Si were formed. It can be concluded that a large amount of fused magnesium was incorporated in the interior of the calcined silica tubes during the high-temperature magnesiothermic reduction process, which led to the formation of nf-Si that maintained their morphology. The diameter of the nf-Si was larger than that of the calcined silica tubes, most likely because of the abundance of space between the silicon nanoparticles. The silicon nanoparticles in the nf-Si@C composite were covered by a thin layer of carbon, and the carbon content calculated by thermogravimetry was 30.2 wt.% (see supporting information, Figure S1); moreover, the thickness of the carbon layer was ~5 nm (Fig. $2d_2$). The nanoparticles in the nf-Si@C were larger than those in the nf-Si (Fig. $2c_2$) because of the growth of the silicon crystal during the high-temperature CVD process (800 °C), as also indicated by the XRD patterns (Fig. 3).

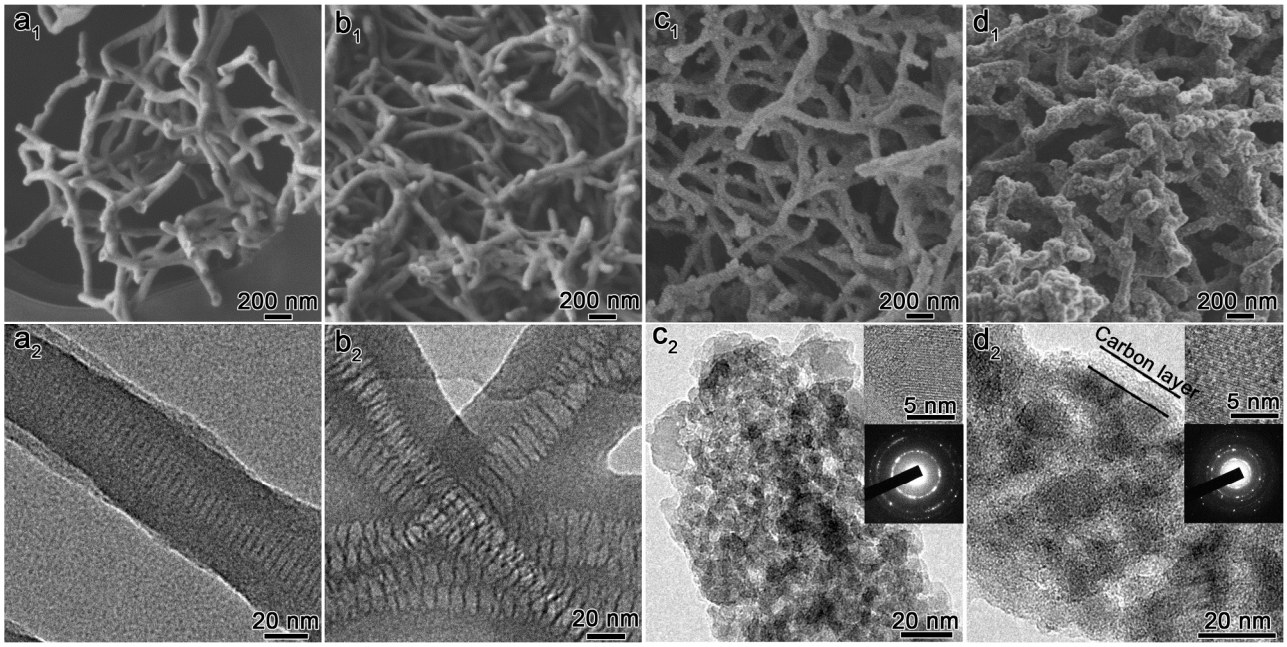

Fig. 2 SEM and TEM images of the as-synthesised silica nanotubes synthesised using a bolaform surfactant (a), the calcined silica nanotubes (b), the silicon nanofibres formed by etching the magnesium oxide (c) and the silicon nanofibres coated with carbon by the CVD method (d).

Figure 3 presents the low- (A) and high-angle (B) XRD patterns of the five samples: (a) as-synthesised lamellar mesoporous silica nanotubes, (b) the calcined mesoporous silica nanotubes, (c) the intermediate product after magnesiothermic reduction, (d) nf-Si and (e) nf-Si@C. As shown in Figure 3A, the as-synthesised silica nanotubes (Fig. 3a) exhibit two well-

resolved peaks at 2θ = 1.9° and 3.8°, which were indexed as the 1st- and 2nd-order reflections of the lamellar structure with a *d*-spacing of 4.6 nm. Based on the molecular length of the surfactant (~3.4 nm), the distance from the amino group to the alkyl carbon atom of APS (--0.3 nm) and the silica wall thickness (see supporting information,Fig. S2), it can be estimated that the lamellar structure was formed by the single-layer arrangement of the bolaform surfactant molecules. It should be noted that the benzene rings in the middle of the silica layered structures (1/2 unit cell) exhibited a higher electron density than the alkyl chains did. Furthermore, the very thin lamellar silica wall led to a weak electron cloud density, and the differences in electron density between the benzene rings and silica layers were small. Thus, the intensity of the 2nd-order reflection was enhanced. If the electron density of the benzene rings were equal to the electron density of the silica layer, the first peak of the XRD pattern would disappear [27, 28] (see supporting information, Fig. S3). The calcined silica nanotubes (Fig. 3b), the intermediate product obtained after the magnesiothermic reduction (Fig. 3c), nf-Si (Fig. 3d) and nf-Si@C (Fig. 3e) showed no peaks in their low-angle XRD patterns, indicating that the lamellar structure was destroyed after removing the surfactant.

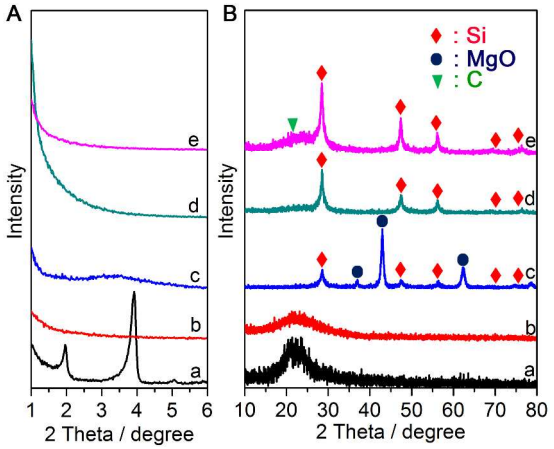

Fig. 3 Low- (A) and high-angle (B) XRD patterns of as-synthesised lamellar-structured mesoporous silica nanotubes (a), the calcined mesoporous silica nanotubes (b), the intermediate product obtained after the magnesiothermic reduction (c), nf-Si (d) and nf-Si@C (e).

Figure 3B shows the high-angle XRD patterns of the samples shown in Figure 3A, and Figure 3Ba and 3Bb show the broad peak obtained over the range of 18°-25°, indicating that the walls of the nanotubes were composed of noncrystalline silica. Figure 3Bc shows the intermediate product obtained after the magnesiothermic reduction process. The peaks at 28°, 47°, 56°, 69° and 76° can be indexed to the (111), (220), (311), (400) and (331) planes of Si crystals, respectively, and the other peaks are attributed to magnesium oxide. Figure 3Bd shows the XRD pattern of the product obtained after etching the magnesium oxide of the mesoporous nf-Si, in which only peaks attributed to crystalline were formed, indicating that the magnesium oxide was removed completely, and finally the well-crystalline silicon was obtained by the mechanochemical reaction process. The enhanced silicon peak intensity of the nf-Si@C (Fig. 3Be) relative to the corresponding peak intensity observed in the pattern of mesoporous nf-Si might be attributed to the growth of the silicon crystal at high temperature, which corresponds with the TEM results. The broad peak at ~23° indicates the existence of a carbon phase.

Figure 4 presents the N_2 adsorption-desorption isotherms (A) and pore-size distribution curves (B) of the mesoporous nf-Si (a) and nf-Si@C (b). As shown in Figure 4a, the N_2 sorption isotherms of nf-Si exhibit representative type IV curves with a sharp capillary condensation step over the relative pressure range 0.65-0.98, which confirm the existence of uniform pores. The Brunauer-Emmett-Teller (BET)-specific surface area and the total pore volume of nf-Si are 291.4 m^2g^{-1} and 0.822 cm^3g^{-1}, respectively. The pore-size distribution calculated by the Barrett-Joyner-Halenda (BJH) method based on the desorption branch of the isotherms indicates a mesopore size of 6.8 nm; the mesopores formed in the silicon nanofibres are attributed to the removal of the template and the volume occupied by the magnesium oxide, which is formed under the magnesiothermal reduction process. Compared with those of nf-Si, the N_2 sorption isotherms and pore-size distribution curves of nf-Si@C shown in Figure 4b indicate a lower BET-specific surface area (144.4 m^2g^{-1}), smaller total pore volume (0.356 cm^3g) and smaller mesopore size (5.3 nm). These disparities are attributed to the growth of the silicon crystal leading to volume shrinkage during the CVD process. Furthermore, a portion of the pore volume was occupied by the carbon coating layer.

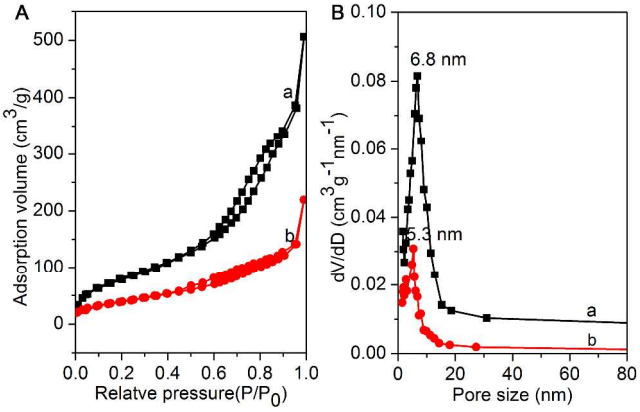

Fig. 4 (A) N_2 isotherms and (B) pore-size distribution of the mesoporous nf-Si (a) and nf-Si@C (b).

Figure 5a compares the cycle capacity and stability of nf-Si and nf-Si@C, and also shows the coulombic efficiency of the nf-Si@C. The nf-Si electrode shows a higher initial capacity of 1669 mAh g^{-1}; however, the capacity drops after several cycles, and the capacity retention at the 100th cycle is 42.7% relative to the capacity at the 2nd cycle. The nf-Si@C electrode shows high

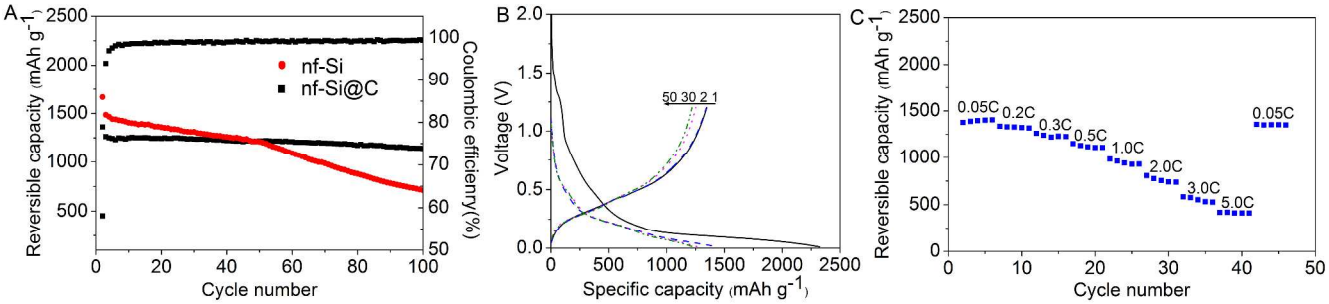

Fig. 5 (a) Cycling performance of nf-Si and nf-Si@C electrodes at 0.05 C (the 1st cycle) and 0.2 C. (b) Voltage profiles of nf-Si@C at 0.05 C (the 1st cycle) and 0.2 C. (C) The reversible capacities of nf-Si@C cycled at different current rates.

electrochemical reversibility, and 84.6% of its original capacity can be retained under the same conditions. Moreover, the coulombic efficiency approaches 99.4%, which demonstrates that the carbon coating is necessary to maintain the cycling stability. Figure 5b shows the voltage profiles of the nf-Si@C electrode at a rate of 0.05 C in the first cycle for electrode activation and at 0.2C in the following cycles. The nf-Si@C electrode delivers capacities of 2324 and 1348 mAh g^{-1} over the first discharge and charge cycles with a coulombic efficiency of 58.0%. The irreversible capacity loss is mainly attributed to the high amorphous carbon content and the solid electrolyte interface (SEI) film formation. Figure 5c shows that as the current rate increases from 0.05 C to 5 C, the capacity declines from 1394 to 414 mAh g^{-1}, and when the current rate finally returns to 0.05 C, a capacity of 1350 mAh g^{-1} is recovered. Here, the 1C is equal to 1350 mA g^{-1}, and the C rate is defined according to practically available maximum specific capacity at 0.05C. The mass loading of the active material on electrodes is approximately 0.5mg cm^{-2}.

Conclusions

In summary, earthworm-like, lamellar-structured silica nanotubes were synthesised by using a rigid bolaform template through the co-structure directing agent method. The nf-Si@C composite obtained after the reduction of the calcined silica nanotubes and the CVD process displayed a stable capacity of approximately 1141 mAh g^{-1} over 100 cycles at 0.2 C and high rate capability. The results suggest that the carbon-deposited silicon nanostructures derived from ordered mesoporous silica are promising candidates for anode materials in high-performance lithium-ion batteries.

Acknowledgements

This work was supported by the 973 project (2013CB934101), the National Natural Science Foundation (21201120, 21101106) of China, the Youth Natural Science Foundation of Shanghai (12ZR1445100) and Evonik Industries.

Notes and references

1. F.-F. Cao, Y.-G. Guo and L.-J. Wan, *Energy Environ. Sci.*, 2011, 4, 1634-1642.
2. J. Li, C. Daniel and D. Wood, *J. Power Sources*, 2011, 196, 2452-2460.
3. J. B. Goodenough and Y. Kim, *Chem. Mater.*, 2010, 22, 587-603.
4. H. Kim, M. Seo, M. H. Park and J. Cho, *Angew. Chem. Int. Ed.*, 2010, 49, 2146-2149.
5. J. R. Szczech and S. Jin, *Energy Environ. Sci.*, 2011, 4, 56-72.
6. J. Yang, B. Wang, K. Wang, Y. Liu, J. Xie and Z. Wen, *Electrochem. Solid-State Lett.*, 2003, 6, A154-A156.
7. J. Xiao, W. Xu, D. Wang, D. Choi, W. Wang, X. Li, G. L. Graff, J. Liu and J.-G. Zhang, *J. Electrochem. Soc.*, 2010, 157, A1047-A1051.
8. T. Song, J. Xia, J.-H. Lee, D. H. Lee, M.-S. Kwon, J.-M. Choi, J. Wu, S. K. Doo, H. Chang, W. I. Park, D. S. Zang, H. Kim, Y. Huang, K.-C. Hwang, J. A. Rogers and U. Paik, *Nano Lett.*, 2010, 10, 1710-1716.
9. H. Jia, P. Gao, J. Yang, J. Wang, Y. Nuli and Z. Yang, *Adv. Energy Mater.*, 2011, 1, 1036-1039.
10. H. K. Liu, Z. Guo, J. Wang and K. Konstantinov, *J. Mater. Chem.*, 2010, 20, 10055-10057.
11. D. Ahn and R. Raj, *J. Power Sources*, 2011, 196, 2179-2186.
12. Y.-X. Yin, S. Xin, L.-J. Wan, C.-J. Li and Y.-G. Guo, *J. Phys. Chem. C*, 2011, 115, 14148-14154.
13. S. H. Ng, J. Wang, D. Wexler, S. Y. Chew and H. K. Liu, *J. Phys. Chem. C*, 2007, 111, 11131-11138.
14. M. Holzapfel, H. Buqa, W. Scheifele, P. Novák and F.-M. Petrat, *Chem. Commun.*, 2005, 1566-1568.
15. C. K. Chan, H. Peng, G. Liu, K. McIlwrath, X. F. Zhang, R. A. Huggins and Y. Cui, *Nature nanotechnology*, 2008, 3, 31-35.
16. L. Hu, H. Wu, Y. Gao, A. Cao, H. Li, J. McDough, X. Xie, M. Zhou and Y. Cui, *Adv. Energy Mater.*, 2011, 1, 523-527.
17. C. K. Chan, R. N. Patel, M. J. O'Connell, B. A. Korgel and Y. Cui, *ACS Nano*, 2010, 4, 1443-1450.
18. S. H. Ng, J. Wang, D. Wexler, K. Konstantinov, Z. P. Guo and H. K. Liu, *Angew. Chem. Int. Ed.*, 2006, 45, 6896-6899.
19. Y. Yao, M. T. McDowell, I. Ryu, H. Wu, N. Liu, L. Hu, W. D. Nix and Y. Cui, *Nano Lett.*, 2011, 11, 2949-2954.
20. H. Wu, G. Chan, J. W. Choi, I. Ryu, Y. Yao, M. T. McDowell, S. W. Lee, A. Jackson, Y. Yang and L. Hu, *Nature nanotech*, 2012, 7, 310-315.
21. J. Cho, *J. Mater. Chem.*, 2010, 20, 4009-4014.
22. C. Du, C. Gao, G. Yin, M. Chen and L. Wang, *Energy Environ. Sci.*, 2011, 4, 1037-1042.
23. J. Song, M. Zhou, R. Yi, T. Xu, M. L. Gordin, D. Tang, Z. Yu, M. Regula and D. Wang, *Adv. Funct. Mater.*, 2014.
24. R. Yi, F. Dai, M. L. Gordin, S. Chen and D. Wang, *Adv. Energy Mater.*, 2013, 3, 295-300.
25. D. Zhao, J. Feng, Q. Huo, N. Melosh, G. H. Fredrickson, B. F. Chmelka and G. D. Stucky, *Science*, 1998, 279, 548-552.
26. S. Che, Z. Liu, T. Ohsuna, K. Sakamoto, O. Terasaki and T. Tatsumi, *Nature*, 2004, 429, 281-284.
27. K. Lund, N. Muroyama and O. Terasaki, *Micropor. Mesopor. Mater.*, 2010, 128, 71-77.

28. D. Xu, Y. Ma, Z. Jing, L. Han, B. Singh, J. Feng, X. Shen, F. Cao, P. Oleynikov and H. Sun, *Nature. Commun*, 2014, 5. DOI: 10.1038/ncomms5262

5

TOC

Carbon-coated mesoporous silicon nanofibres for use in advanced lithium-ion batteries shows a stable capacity of approximately 1141 mAh g^{-1} over 100 cycles at 0.2 C.